

LHC Triggers using FPGA Image Recognition

J. Brooke^{1*}, E. Clement¹, M. Glowacki^{1,2}, S. Paramesvaran¹, J. Segal¹

¹H H Wills Physics Laboratory, University of Bristol, Tyndall Avenue, Bristol, BS8 1TL, United Kingdom.

²CERN, Esplanade des Particules 1, 1211 Geneva, 23, Switzerland.

*Corresponding author(s). E-mail(s): james.brooke@bristol.ac.uk;

Contributing authors: emyr.clement@bristol.ac.uk; maciej.mikolaj.glowacki@cern.ch; sudarshan.paramesvaran@bristol.ac.uk; jeronimo.segal@bristol.ac.uk;

Abstract

The implementation of convolutional neural networks in programmable logic, for applications in fast online event selection at hadron colliders is studied. In particular, an approach based on full event images for classification is studied, including hardware-aware optimisation of the network architecture, and evaluation of physics performance using simulated data. A range of network models are identified that can be implemented within resources of current FPGAs, as well as the stringent latency requirements of HL-LHC trigger systems. A candidate model that can be implemented in the CMS L1 trigger for HL-LHC was shown to be capable of excellent signal/background discrimination, although the performance depends strongly on the degree of pile-up mitigation possible prior to image generation.

Keywords: Particle physics, Machine learning, Convolutional neural network, Field programmable gate array, Trigger, Data-acquisition

1 Introduction

Online event selection is a major experimental challenge at the Large Hadron Collider (LHC) [1]. The LHC general purpose detectors [2, 3] require on-detector data buffers, due to their 4π coverage and material budget constraints, and therefore require a fast, $\mathcal{O}(\mu\text{s})$, trigger signal to initiate readout. The physics performance of these trigger systems, in terms of signal efficiency and trigger rate, must be exceptional, given the challenge of searching for low cross-section physics at increasingly high instantaneous luminosity and large numbers of simultaneous proton-proton interactions, known as pile-up (PU). These trigger systems are currently constructed from custom electronics boards using Field Programmable Gate

Array (FPGA) technology, communicating via high bandwidth optical links [4, 5]. Typically, the logic implemented in the trigger performs a crude reconstruction of the collision, starting with detector level information and building up to physics objects such as leptons and jets, which are then used to select events by placing requirements on transverse momentum and other such criteria.

The trigger systems currently employed by the ATLAS and CMS experiments feature a hardware first-level system which receives reduced granularity data from the detector at the full LHC bunch-crossing rate (40 MHz) and processes this to generate a trigger decision [4, 5]. In both cases this Level-1 (L1) trigger comprises custom electronics based around high-bandwidth optical links and programmable logic (FPGA) devices, upon

which reconstruction and selection algorithms are implemented. The current L1 trigger systems at ATLAS and CMS must generate a decision within a latency of $\mathcal{O}(4\mu\text{s})$ and with a maximum accept rate of $\mathcal{O}(100\text{kHz})$.

These requirements will be evolving as the next phase of the LHC begins in 2030. The High Luminosity LHC (HL-LHC) [6] will deliver an order of magnitude more data to the experiments, with up to 200 PU. In order to prepare for this unprecedented amount of data, experiments must refine and upgrade their online data selection systems. Allowed latencies will increase along with the output rate of the system, but even this is insufficient alone to cope with the data challenge, and hence newer more sophisticated techniques are being explored. Furthermore, even with future technological advances, low latency trigger systems appear to be essential at future hadron colliders. This need is driven by the readout link bandwidth from the central detectors, which is constrained by power and cooling limitations. Unless substantial advances are made in link power consumption, the need for low latency triggers is foreseen at the next proposed hadron collider, the Future Circular Collider (FCC-hh) [7]. The physics performance of future hadron colliders may therefore be substantially driven by the capabilities of off-detector trigger systems, which will likely use extremely advanced processing compared with current systems.

In terms of data processing algorithms for online event selection, the use of machine learning (ML) is a highly active area. Machine learning has been ubiquitous in offline analysis at collider experiments for many years, with increasing adoption in software-based online selection systems. Recent work has included firmware-based implementations of ML algorithms, which facilitate applications in ultra-low latency triggers. The implemented algorithms include neural networks [8–18], autoencoders [19–21], boosted-decision trees [22] and transformers [23].

In this paper, we explore the use of simple computer vision methods to classify proton-proton interactions for use in hardware trigger systems at the HL-LHC. We transform detector data into 2D images, which are then processed by convolutional neural networks (CNNs).

Image classification is a mature problem in the space of computer vision; deep learning models

capable of image classification can compete to outperform each other on the largest visual database ever assembled, *imageNet* [24]. There are two key characteristics of CNNs which are responsible for their impressive performance. First, the convolution operation exploits translational invariance by utilising shared kernels across the whole image, enabling weights to be derived from all locations on the input. Secondly, CNNs learn spatial hierarchies of patterns. A first convolutional layer will learn small local patterns such as edges, a second convolutional layer will learn larger patterns made of the features of the first layers, and so forth. This allows CNNs to efficiently learn increasingly complex and abstract visual concepts.

This paper is arranged as follows; in Section 2 we discuss how the images could be generated within the HL-LHC L1 trigger systems, then in Section 3 we detail how we simulated such images for this study. Section 4 provides an overview the CNN model architecture, and Section 5 discussed hardware specific optimisations of the network. In Section 6 we present the physics performance of this approach and in Section 7 we summarise the key findings of this study.

2 Image Generation in HL-LHC Triggers

In preparation for the HL-LHC, both ATLAS and CMS will upgrade their trigger and data-acquisition systems to handle the extremely challenging environment of 200 PU. These upgrades include use of detector information not currently available in the hardware trigger - for example, inclusion of tracking at 40 MHz in the CMS L1 trigger. They will also facilitate use of larger FPGAs, and the latest FPGA technology, for example, use of Xilinx Versal in the ATLAS L0 global processor [25]. Inter-board communication will use link speeds of up to 25Gbps. Finally, advanced data processing architectures such as time-multiplexing are planned for both CMS and ATLAS. This architecture segments the detector inputs to the trigger systems by bunch crossing, sending information from consecutive crossings to consecutive nodes in a round-robin fashion. This allows algorithms to be implemented which rely on data from the full detector (such as CNNs), as well as accommodating algorithms requiring relatively

long latency. As an example, the CMS L1 trigger architecture for HL-LHC is shown in Figure 1.

The hardware trigger architecture for both CMS and ATLAS at HL-LHC provide several opportunities for representation of events as a 2D image. Perhaps most obviously, data from the calorimeters is typically segmented into trigger towers in pseudorapidity η and azimuthal angle ϕ , and the transverse energy E_t is reported for each tower. This data is easily represented as 2D image for each bunch crossing, with pixel coordinates indicating η and ϕ and pixel brightness representing E_t . Such images are easily and quickly generated, but will include energy from all pile-up events at nominal HL-LHC conditions. Images with significantly reduced pile-up can be generated in the CMS Correlator Trigger (CT). Here, data from the calorimeter, muon and tracking detectors are brought together, allowing a fast version of the particle flow algorithm to be applied, followed by the pile-up per particle (PUPPI) pile-up rejection algorithm. The resulting particle flow candidates for a given bunch crossing can be histogrammed to give a 2D image representation of the event, potentially with more flexibility on the η and ϕ segmentation, but again with pixel brightness representing the transverse energy.

3 Simulated Images

To quantify the potential performance of ML image classification in these contexts, we generated several image datasets that represent example signal and background images produced at the HL-LHC. Signal events were produced by simulating di-Higgs production, with both Higgs bosons decaying to a pair of b quarks. The matrix element calculations were performed with MADGRAPH5_aMC@NLO v2.9.9 [27, 28], at NLO accuracy in QCD. PYTHIA 8 v8.305 [29] was then used for the simulation of the parton shower, hadronization, and underlying event. Background events were produced by simulating minimum bias events, where a proton-proton interaction results only in soft multiple-parton interactions, using PYTHIA 8. The detector response was then simulated using DELPHES v3.5.0 [30–32], which provides a parameterised description of the response of the CMS detector.

The impact of pile-up was simulated in DELPHES by overlaying each event with a Poisson-distributed random number of minimum bias events. Samples were generated with a mean number of 60, 140, and 200 minimum bias events overlaid. Background events were generated, comprising only the overlaid pile-up interactions, i.e. without the inclusion of the signal HH process, corresponding to a typical bunch crossing in the CMS detector.

Images were then generated from the simulated calorimeter towers, which in CMS correspond to the sum of energy deposited in a group of 5x5 electromagnetic calorimeter (ECAL) cells and the hadronic calorimeter cell that is aligned with the ECAL cells. Images were generated by forming a two-dimensional (2D) histogram in η - ϕ of the transverse energy (E_T) deposited in each calorimeter tower. Only the region $|\eta| < 3$ was included, since this is region for which PU rejection is expected to be effective. The towers have a size of 0.087×0.087 in η - ϕ , giving a default image size of $72\eta \times 72\phi$ pixels.

A total of 64k signal events and 64k background events were generated to train the models, and a further 16k each of signal and background events are used as a validation sample during the training procedure. A further independent dataset comprising of 20k signal events and 200k background events are used for testing the physics performance of the models. A significantly larger background sample is used in this case to accurately test background rejection rates of the order of 10^{-4} .

We also generated samples to explore the advantage of using pile-up subtracted data for image generation, such as may be obtained from the CMS CT. We performed a crude pile-up rejection within the DELPHES simulation by randomly rejecting, with fixed probability, particles that originate from pile-up interactions before they are included in the simulated calorimeter response. Two samples were generated, starting from the 200 PU signal and background samples, with rejection probabilities of 30% and 70%. These samples do not attempt to simulate the PUPPI algorithm, rather they allow us to quantify the impact of pile-up rejection ahead of image recognition.

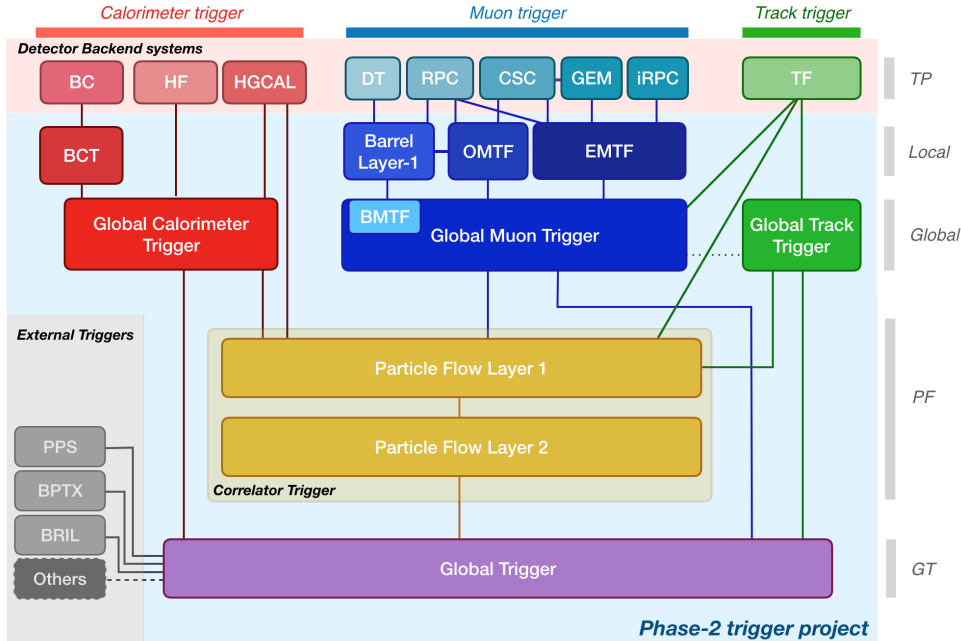


Fig. 1: The CMS L1 trigger architecture for HL-LHC [26].

Example images are shown in Figure 2, for HH(bbbb) and min-bias processes with 200 pile-up, for image sizes of 72×72 and 12×12 .

4 Network Architecture

Our approach relies on classification of images as either signal or background using a CNN. The CNN architectures studied here share a similar design, which is shown schematically in Figure 3, and are composed of two modules. The first module, tasked with feature extraction, consists of two convolutional layers, each followed by a ReLU activation function for non-linearity. Following the feature mapping performed by the convolutional layers, the output tensor is flattened and passed to a fully connected network consisting of three layers with 32, 16 and 8 neurons respectively. Each fully connected layer is again followed by a non-linear ReLU activation function. Finally, a single neuron output layer is used for binary classification, with the output score being translated to a probability distribution by the sigmoid activation function. The model architectures being studied differ in the size, or granularity, of the inputs images; the size of the kernel in the first convolutional layer; the stride of the kernel in the first convolutional layer;

and the number of filters in the first convolutional layer. The architecture of the second convolutional layer is the same for all models considered, and comprises of one kernel of size three, with a stride of one.

When training image recognition networks, gradient descent convergence and numerical stability is greatly improved if all images have pixel values in the range $[0,1]$. Due to the wide dynamic range of the E_T of particles entering our detector simulation, and hence the pixels in our images, we first saturate images to a maximum E_T value before scaling to the $[0,1]$ range. The value for saturating the pixel E_T was set to 512 GeV, which was found to maximise the performance of the models based on the metrics defined in Section 6.

Another consideration that has to be addressed is the discontinuity of unrolling cylindrical geometries to form 2D images; after this procedure the model is not intrinsically aware that opposing edges in the ϕ plane are connected. Events where physics level object with a typical size of many pixels, such as jets, populate the edges of the images in the ϕ dimension can cause misclassification of the event. To circumvent this, input images are padded by translating three pixel columns from one side of the image to the

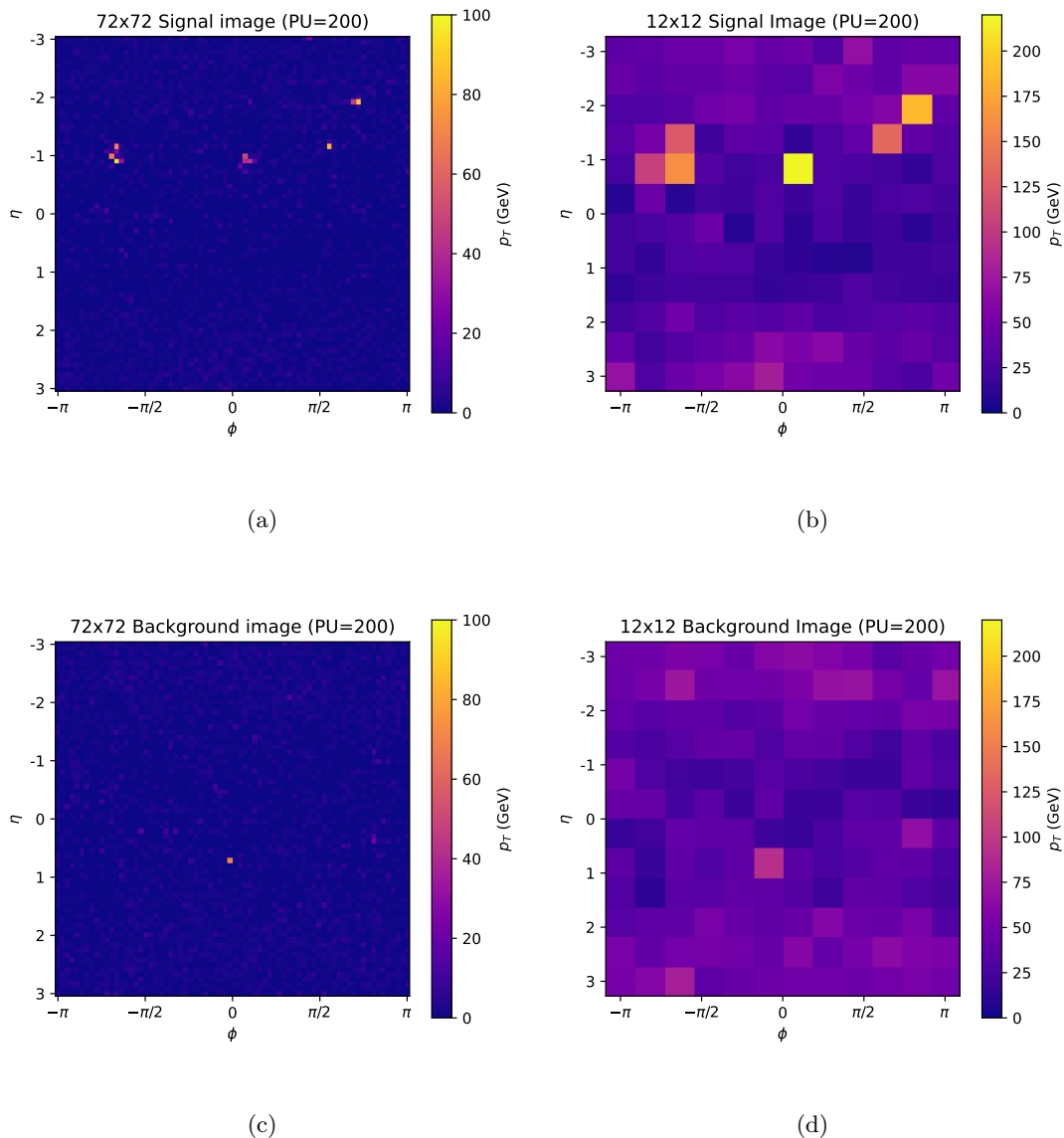


Fig. 2: Example images used for model training and evaluation, for 200 PU. A signal HH(bbbb) image is shown at a) 72×72 pixel resolution, and b) 12×12 pixel resolution. A background image is shown with c) 72×72 pixel resolution, and d) 12×12 pixel resolution.

opposing side. This choice ensures that a jet that is centred near the edge of the image in ϕ is represented at least once within the padded image. Finally, to allow the convolution kernel to be centred on edge pixels, the images are zero-padded in the η plane.

The models are implemented and trained using the Keras API [33]. The training was performed

using the ADAM optimiser [34], with the binary cross entropy as the loss function being minimised.

As the models are targeting deployment on an FPGA, we employ quantisation-aware training to ensure that fixed-point arithmetic is taken into account during the training procedure. The QKeras package [35] is used to implement the quantised models, and the weights of all layers

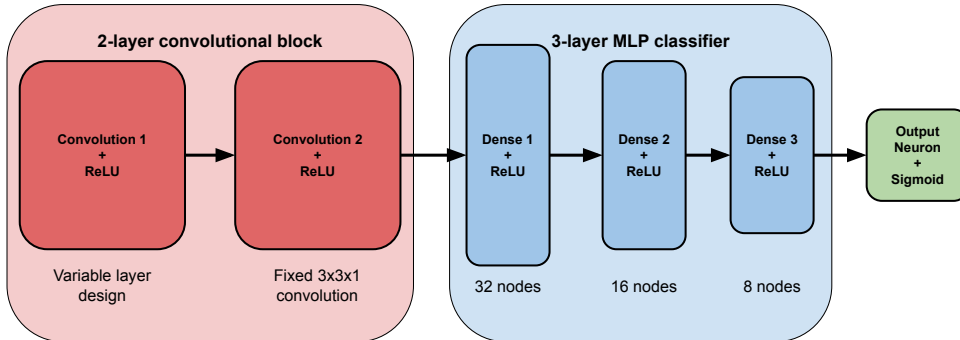


Fig. 3: A schematic of the model architectures under study. The convolutional layers are shown in red, and the fully connected layers are shown in blue. The parameters of the fully connected layers and the second convolutional layer are the same for all model architectures, whereas the parameters of the first convolutional layer, and the size of the inputs, differ for each model.

except the final layer are quantised to a precision of 8 bits in total, with 2 integer bits. The output node and the final sigmoid layer utilizes a larger number of bits, 16 in total, to maintain precision in the output score. The performance of the quantised model with this level of quantisation is found to have the same performance as a model utilising floating-point arithmetic. To prevent overfitting, the training is halted when the loss function calculated on the validation set is no longer decreasing over a set amount of epochs.

The choice of quantisation places a significant restriction on the magnitude of the weights that can be learned. Weights were prevented from growing too large, and potentially exceeding the maximum representable value, by adding a term to the loss function that is proportional to the magnitude of the weight squared, i.e. L2 regularization. A regularization strength of 10^{-5} was found to provide sufficient regularization without sacrificing model performance.

The HLS4ML package [8, 10, 36, 37] is used to convert the model architecture and the corresponding weights into Vivado HLS code, which is in turn synthesised into VHDL code. Estimates of the resource usage of a model implemented on a given FPGA are provided by this synthesis, along with the latency and initiation interval (II), where II is defined as the period of time after which the model can accept data from a new event. An implementation of *im2col* [10, 37, 38] within HLS4ML is utilised, allowing multiple

convolution operations to be performed in parallel. This reduces the latency and the II of the model when compared to a firmware implementation that accepts a single bin as an input on each clock cycle, at a cost of increased firmware resource usage. The level of parallelization is chosen to meet the firmware constraints that will be described in Section 5.

5 Hardware Aware Model Optimisation

In order to assess whether FPGA implementation of a network is feasible, we must assume a particular application. For this study, we assume images are generated in the CMS CT, where the target FPGA is the Xilinx VU9P. We require the network to be implementable on a single Super Logic Region (SLR) of this FPGA, corresponding to approximately one third of the total logic available. We also assume the CT has a time-multiplexing period of 6 bunch-crossings, which corresponds to a maximum II of 54ns for our models. To explore the model design space that can be accommodated in the target FPGA and meet the constraints set by the chosen application, we scan a range of networks with different parameters and consider those that meet the criteria on the II and resource usage.

The primary parameter varied for the scan of potential networks was the input image resolution. Higher-resolution images offer more detailed

information about the event, but also quadratically increase the computational cost of the first convolutional layer in our models and the II of the models. The kernel size and stride of the kernel in the first convolutional layer were adjusted based on the input resolution to meet the constraints. Increasing the kernel size and stride will reduce the firmware resources of a model by reducing the number of instances of filters that are computed in a convolutional layer, which also reduces the II of the model. The II of the models can also be tuned by the parallelisation factor of the first convolutional layer in the im2col implementation of CNNs in HLS4ML. We chose the level of parallelization such that one row of outputs from the first convolutional layer is calculated on each clock cycle, which typically results in architectures that are able to satisfy the firmware requirements. For some combinations of image granularity, number of kernels and their size and stride, this choice of parallelization factor may yield a model that does not satisfy the criteria we have set on the firmware size and II of the models, whereas other choices may meet those criteria. Models based on the same network configuration, but with different parallelization factors, will have identical physics performance. These models were also not found to outperform the best performing models when using our default choice of parallelization factor, and are therefore not considered further. Additionally, the number of filters in the convolutional layers was varied when the rest of the network was estimated to be small enough to allow for it.

By varying the parameters of the models, we obtain an initial shortlist of 16 networks, for which resource usage and II were estimated using HLS4ML and Vivado HLS. The estimated LUT usage and II for these models are shown in Figure 4. In this initial scan over the network architecture space, the networks are not trained. Whilst pruning the models during training could reduce their LUT usage, the II would remain unchanged. As several architectures are already found to satisfy the firmware constraints without pruning, we do not consider the effect of pruning on the resource usage in this study.

The 11 networks conforming to the firmware constraints we set out are shown in green in Figure 4 and are listed in detail in Table 1. For these models, the flip-flop (FF) usage ranges from

4% to 9% (with respect to the total within an SLR). Block RAM usage is no more than 27% of an SLR, with many models only using a single BRAM. The latency of these models ranges from 228ns to 397ns, with models using fewer LUTs typically having a lower latency, and vice versa.

We note that the II decreases from 24 clock cycles for Model 1, to 18 clock cycles for both Models 2 and 3. These three models are based on the same image size, kernel size and stride in the first convolutional layer, and are expected to have the same II, even though the number of filters in this layer differ. This indicates that a different choice was made during the synthesis of Model 1 into VHDL, compared to the other two models.

A few models shown in red in Figure 4, and also listed in Table 1, do not meet the hardware constraints. Models 12-14 satisfy the criterion on the II, but the LUT usage is greater than the requirement. Whilst the LUT could be reduced by pruning, or by other model compression techniques, these models are not considered further in this study, given that at least one other model based on the same image sizes does satisfy the hardware constraints. Model 15 is based on the lowest resolution images we consider, and is an attempt at constructing a model that meets the hardware constraints where the kernels in the first convolutional layer have a stride of one. For this model, it was necessary to include an additional max pooling layer between the first and second convolutional layers to reduce the dimensions of the features being propagated further along the model, and hence the resource usage. Whilst this additional step results in a model that meets the criterion on the resource usage, the II of this model is too large. Model 16, which is the model with the largest II and resource usage, corresponds to a model based on the maximum image size that is closest to meeting the firmware criteria, and uses a relatively large kernel size, the largest possible stride to ensure all pixels in the image are seen by the model, and only a single filter. Whilst it was not expected for such model to satisfy the hardware constraints, this model will be used in Section 6 when considering the physics performance of our models.

Table 1: LUT usage and II of various models with different input image resolutions, kernel size, stride and number of filters in the first convolutional layer. The resource usage estimates and II are obtained with HLS4ML, with the Xilinx VU9P as the target FPGA. The LUT usage is quoted with respect to the total within an SLR. Models 1-11 satisfy the hardware constraints described in the text, whereas Models 12-16 do not.

Model label	Image size (padded)	Kernel size	Stride	Filters	Params	LUT (% of SLR)	II	Latency (ns)
1	18	3	3	1	1237	42.5	24	228
2	18	3	3	2	1256	44.4	18	244
3	18	3	3	4	1294	53.9	18	283
4	18	4	2	1	1884	75.0	36	356
5	18	6	2	1	1552	59.4	21	317
6	24	3	3	1	1877	68.0	32	311
7	24	4	4	2	1270	46.7	30	292
8	24	6	3	1	1552	59.7	28	325
9	30	5	5	1	1253	52.2	18	283
10	42	7	5	1	1917	79.1	32	397
11	42	7	7	1	1277	64.5	18	303
12	24	6	2	1	2800	116.6	30	311
13	24	8	2	1	2348	106.9	27	419
14	30	3	3	1	2773	105.5	50	444
15	18	5	1	1	1541	91.3	84	450
16	78	8	7	1	3372	219.4	99	739

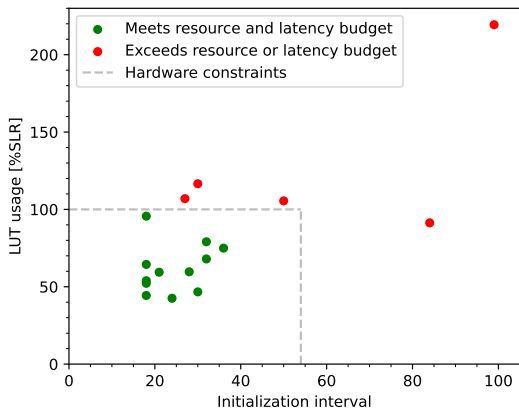


Fig. 4: Estimated LUT usage against II for the initial scan over model architectures. Resource usage is estimated by Vivado HLS. The grey dashed lines indicate maximum values of LUT usage and II which can be accommodated within the target FPGA and application.

6 Physics Performance

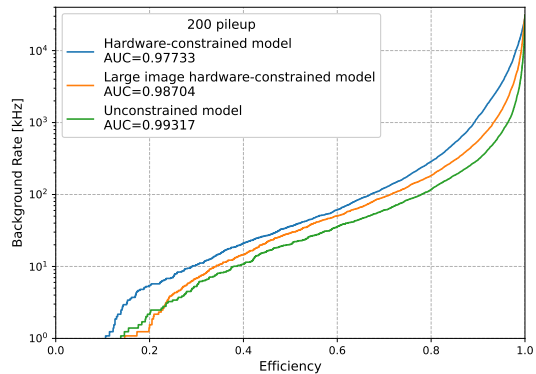
Having determined a set of models which can be accommodated within reasonable firmware

resources, we train those models as described in Section 4. To evaluate their performance, we assume events are selected by the online trigger system if the classification score exceeds a threshold. The L1 trigger rate is then computed as a function of threshold from the sample of min-bias events, while the signal efficiency is computed in the same way from the sample of HH(bbbb) events. The L1 trigger rate and signal efficiencies for our models are calculated at multiple points to construct a receiver operating characteristic (ROC) plot, and the area under the curve (AUC) is calculated to determine the performance of the models over a wide range of trigger rate and signal efficiency, covering several orders of magnitude of L1 trigger rate. We also consider a single comparison point from the ROC curve that reflects a possible working point for such an algorithm. In particular, we choose a point corresponding to the signal efficiency obtained for an L1 trigger rate of 10 kHz, which is comparable to the rate of L1 trigger seeds discussed in Ref. [26] that would target HH(bbbb) events. For Models 1-11, the signal efficiencies for a rate of 10 kHz are found to be comparable and are within the

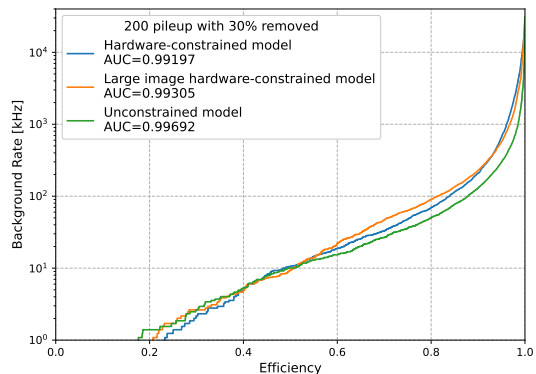
range 26.8% – 31.7% under the 200 PU assumption. These efficiencies are calculated using k -fold cross-validation, with $k = 5$, and the final efficiency for each model was calculated as an average over the five folds to obtain a robust calculation of the signal efficiency at the 10 kHz rate. The best performing model at this comparison point corresponds to Model 3 in Table 1. This model is based on 18×18 pixel images including padding, has a kernel size of three in the first convolutional layer, a corresponding stride of three, and a total of four filters. This model is chosen as the final hardware-constrained model for the following discussion.

We now explore the effect of the hardware-based optimisation on the performance of our model. Figure 5a shows the ROC curves at 200 PU for several different models including the chosen hardware-constrained model (Model 3), a model based on the finest granularity images that comes close to meeting hardware constraints (Model 16), and a model based on finest granularity images that is not constrained. The last of these models uses a single 5×5 filter with a stride of 1 in the first convolutional layer, which would result in greater resource utilisation than is available on the target FPGA and a significantly larger II than models shown in Table 1. Figures 5b and 5c show the ROC results for the same models, under assumptions of 30% pile-up removal and 70% pile-up removal, respectively. To ensure a fair comparison between the performance of these models, they are trained and tested on images that differ in their granularity, but are otherwise identical. As can be seen, the introduction of hardware constraints reduces the AUC for all PU mitigation scenarios. However, for a target L1 trigger rate of 10 kHz, the impact of hardware constraints on achievable signal efficiency is less obvious. With no PU mitigation, increasing constraints reduces efficiency as expected, while for the 70% PU removal scenario the order of the large image models is reversed, and for the 30% PU removal scenario the 3 models achieve comparable performance. This likely results from the model training, which optimises for maximal AUC, rather than efficiency at very high background rejection rates.

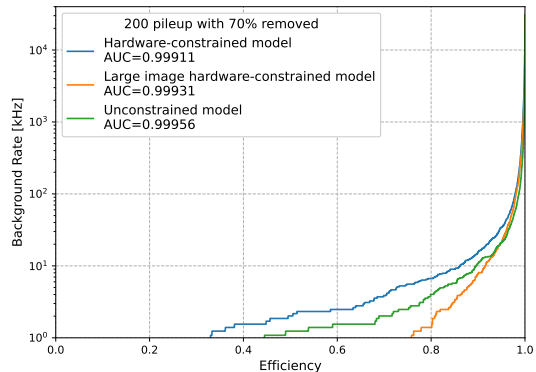
Finally, Figure 6 shows the ROCs for each pileup mitigation scenario for the hardware-constrained model (Model 3) only. In addition, the ROC curve for a model trained using signal



(a)



(b)



(c)

Fig. 5: Receiver operating characteristic (ROC) curves at 200 PU, under different pile-up mitigation scenarios: a) no mitigation, b) 30% removal, c) 70% removal. For each scenario, the ROCs are presented for the hardware-constrained model (Model 3), large image hardware-constrained model (Model 16), and an unconstrained model.

and background images with no pileup overlaid (labelled “1 pileup”), is presented, to indicate the ultimate performance of the CNN approach, equivalent to perfect pileup mitigation. As can be seen, even a modest level of pileup removal can significantly improve the signal efficiency with respect to the no mitigation scenario. Specifically, at a rate of 10 kHz, the signal efficiency increases to $\sim 50\%$ ($\sim 85\%$) for the 30% (70%) pileup removal scenarios. Comparing this increase in efficiency to the $\sim 5\%$ range in efficiencies obtained for the various models shown in Table 1, and also the increase in efficiencies attainable without hardware constraints shown in Figure 5, shows that improving the quality of the inputs to the model through pileup mitigation has a greater effect than simply optimising models within the defined firmware constraints.

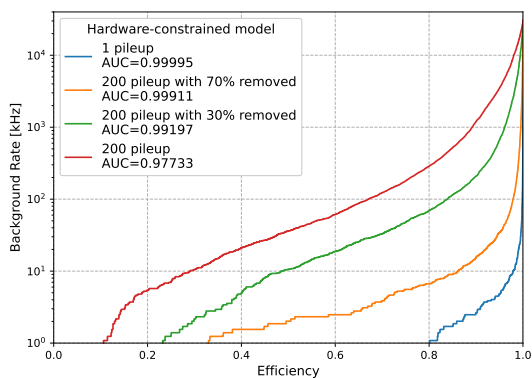


Fig. 6: ROC curves for the hardware constrained model (Model 3), under 4 different pileup scenarios.

7 Conclusions

In this study, we set out to assess the viability of Convolutional Neural Networks implemented in FPGAs, as a method of selecting events of interest at the High Luminosity LHC. We have shown that, provided the image size is sufficiently small, such networks can be implemented in FPGA technology planned for the CMS HL-LHC trigger, with the full network computation being handled within very tight latency constraints associated with the LHC trigger systems. In the absence of

pile-up, candidate networks are capable of excellent signal identification performance. If the input images can be generated after some moderate pileup mitigation is applied, then the performance even at full pile-up can exceed that of conventional trigger algorithms. It should be noted, however, that these studies are limited by the use of fast simulation of the CMS detector, and an extremely simplistic pileup removal algorithm. Further studies using the full detector simulation and realistic pileup mitigation algorithms will be required to fully evaluate the performance of this approach.

Since the approach studied here focusses on a single signal of interest, the bandwidth allocation and resource usage on an FPGA could be considered high, especially as conventional heuristic trigger paths typically use much lower resources per trigger line. However, we have explored a particularly high-value signal, that of di-Higgs production with each Higgs decaying to two bottom quarks. The physics benefits gained from improving selection of such events may outweigh the cost in terms of FPGA resource. Furthermore, as larger FPGAs and more ML-adept toolsets come to market, this should be less of an issue and as such the authors are currently investigating the use of the Xilinx Versal AI Core series cards, along with VitisAI and High-Granularity Quantisation to explore the benefits of this new technology. As future hadron colliders are proposed, such as FCC-hh [39], it will become increasingly important to exploit the use of machine learning for ultra-low latency applications.

Acknowledgements. We acknowledge the Fast Machine Learning collective as an open community of multi-domain experts and collaborators, which has made this work possible. We thank Dr Aaron Bundock for his feedback and help preparing this manuscript. This work was supported by the Science and Technology Facilities Council (grants ST/W000490/1, ST/R005788/1, ST/P006779/1), as well as the Engineering & Physical Sciences Research Council (grant EP/S023992/1).

Author contributions. All authors contributed to the research methodology, discussion of results, and review and editing of the manuscript. JB conceived the project. JB, EC and JS performed simulation. MG and JS trained

and evaluated the models, and JS performed the hardware optimisation. SP supervised the work.

Declarations

Competing Interests The authors have no competing interests to declare.

References

- [1] Bruning, O.S., Collier, P., Lebrun, P., Myers, S., Ostojic, R., Poole, J., Proudlock, P. (eds.): LHC Design Report Vol.1: The LHC Main Ring (2004) <https://doi.org/10.5170/CERN-2004-003-V-1>
- [2] Airapetian, A., et al.: ATLAS: Detector and physics performance technical design report. Volume 1 (1999)
- [3] Bayatian, G.L., et al.: CMS Physics: Technical Design Report Volume 1: Detector Performance and Software (2006)
- [4] Aad, G., et al.: Technical Design Report for the Phase-I Upgrade of the ATLAS TDAQ System (2013)
- [5] The CMS Collaboration: CMS Technical Design Report for the Level-1 Trigger Upgrade (2013)
- [6] Zurbano Fernandez, I., et al.: High-Luminosity Large Hadron Collider (HL-LHC): Technical design report. Technical report (December 2020). <https://doi.org/10.23731/CYRM-2020-0010>
- [7] Abada, A., et al.: FCC-hh: The Hadron Collider: Future Circular Collider Conceptual Design Report Volume 3. Technical Report 4 (2019). <https://doi.org/10.1140/epjst/e2019-900087-0>
- [8] Duarte, J., Han, S., Harris, P., Jindariani, S., Kreinar, E., Kreis, B., Ngadiuba, J., Pierini, M., Rivera, R., Tran, N., Wu, Z.: Fast inference of deep neural networks in fpgas for particle physics. *Journal of Instrumentation* **13**(07), 07027 (2018) <https://doi.org/10.1088/1748-0221/13/07/P07027>
- [9] Nottbeck, N., Schmitt, C., Büscher, V.: Implementation of high-performance, sub-microsecond deep neural networks on FPGAs for trigger applications. *JINST* **14**(09), 09014 (2019) <https://doi.org/10.1088/1748-0221/14/09/p09014> [arXiv:1903.10201](https://arxiv.org/abs/1903.10201) [physics.ins-det]
- [10] Aarrestad, T., et al.: Fast convolutional neural networks on FPGAs with hls4ml. *Mach. Learn. Sci. Tech.* **2**(4), 045015 (2021) <https://doi.org/10.1088/2632-2153/ac0ea1> [arXiv:2101.05108](https://arxiv.org/abs/2101.05108) [cs.LG]
- [11] Iiyama, Y., et al.: Distance-Weighted Graph Neural Networks on FPGAs for Real-Time Particle Reconstruction in High Energy Physics. *Front. Big Data* **3**, 598927 (2020) <https://doi.org/10.3389/fdata.2020.598927> [arXiv:2008.03601](https://arxiv.org/abs/2008.03601) [physics.ins-det]
- [12] Bortolato, G., Cepeda, M., Heikkilä, J., Huber, B., Leutgeb, E., Rabady, D., Sakulin, H.: Design and implementation of neural network based conditions for the CMS Level-1 Global Trigger upgrade for the HL-LHC. *JINST* **19**(03), 03019 (2024) <https://doi.org/10.1088/1748-0221/19/03/C03019>
- [13] Burazin Mišura, A., Musić, J., Prvan, M., Lelas, D.: Towards Real-Time Machine Learning-Based Signal/Background Selection in the CMS Detector Using Quantized Neural Networks and Input Data Reduction. *Appl. Sciences* **14**(4), 1559 (2024) <https://doi.org/10.3390/app14041559>
- [14] Alimena, J., Iiyama, Y., Kieseler, J.: Fast convolutional neural networks for identifying long-lived particles in a high-granularity calorimeter. *JINST* **15**(12), 12006 (2020) <https://doi.org/10.1088/1748-0221/15/12/P12006> [arXiv:2004.10744](https://arxiv.org/abs/2004.10744) [hep-ex]
- [15] Migliorini, M., Pazzini, J., Triossi, A., Zanetti, M., Zucchetta, A.: Muon trigger with fast Neural Networks on FPGA, a demonstrator. *J. Phys. Conf. Ser.* **2374**(1), 012099 (2022) <https://doi.org/10.1088/1742-6596/2374/1/012099> [arXiv:2105.04428](https://arxiv.org/abs/2105.04428) [hep-ex]
- [16] Ospanov, R., Feng, C., Dong, W., Feng,

- W., Zhang, K., Yang, S.: Development of a resource-efficient FPGA-based neural network regression model for the ATLAS muon trigger upgrades. *Eur. Phys. J. C* **82**(6), 576 (2022) <https://doi.org/10.1140/epjc/s10052-022-10521-8> [arXiv:2201.06288](https://arxiv.org/abs/2201.06288) [physics.ins-det]
- [17] The CMS collaboration: Neural network-based algorithm for the identification of bottom quarks in the CMS Phase-2 Level-1 trigger. Technical report (2022). <https://cds.cern.ch/record/2814728>
- [18] Aad, G., *et al.*: Artificial Neural Networks on FPGAs for Real-Time Energy Reconstruction of the ATLAS LAr Calorimeters. *Comput. Softw. Big Sci.* **5**(1), 19 (2021) <https://doi.org/10.1007/s41781-021-00066-y>
- [19] Govorkova, E., *et al.*: Autoencoders on field-programmable gate arrays for real-time, unsupervised new physics detection at 40 MHz at the Large Hadron Collider. *Nature Mach. Intell.* **4**, 154–161 (2022) <https://doi.org/10.1038/s42256-022-00441-3> [arXiv:2108.03986](https://arxiv.org/abs/2108.03986) [physics.ins-det]
- [20] Bhattacharjee, B., Konar, P., Ngairangbam, V.S., Solanki, P.: LLPNet: Graph Autoencoder for Triggering Light Long-Lived Particles at HL-LHC (2023) [arXiv:2308.13611](https://arxiv.org/abs/2308.13611) [hep-ph]
- [21] Theenhausen, H., Krosigk, B., Wilson, J.S.: Neural-network-based level-1 trigger upgrade for the SuperCDMS experiment at SNO-LAB. *JINST* **18**(06), 06012 (2023) <https://doi.org/10.1088/1748-0221/18/06/P06012> [arXiv:2212.07864](https://arxiv.org/abs/2212.07864) [physics.ins-det]
- [22] Summers, S., *et al.*: Fast inference of Boosted Decision Trees in FPGAs for particle physics. *JINST* **15**(05), 05026 (2020) <https://doi.org/10.1088/1748-0221/15/05/P05026> [arXiv:2002.02534](https://arxiv.org/abs/2002.02534) [physics.comp-ph]
- [23] Jiang, Z., Yin, D., Khoda, E.E., Loncar, V., Govorkova, E., Moreno, E., Harris, P., Hauck, S., Hsu, S.-C.: Ultra Fast Transformers on FPGAs for Particle Physics Experiments (2024) [arXiv:2402.01047](https://arxiv.org/abs/2402.01047) [cs.LG]
- [24] Deng, J., Dong, W., Socher, R., Li, L.-J., Li, K., Fei-Fei, L.: Imagenet: A large-scale hierarchical image database. In: 2009 IEEE Conference on Computer Vision and Pattern Recognition, pp. 248–255 (2009). <https://doi.org/10.1109/CVPR.2009.5206848>
- [25] Qian, W.: A full-function Global Common Module prototype for ATLAS Phase-II upgrade. *JINST* **19**(02), 02049 (2024) <https://doi.org/10.1088/1748-0221/19/02/C02049>
- [26] Zabi, A., Berryhill, J.W., Perez, E., Tapper, A.D.: The Phase-2 Upgrade of the CMS Level-1 Trigger (2020)
- [27] Alwall, J., Frederix, R., Frixione, S., Hirschi, V., Maltoni, F., Mattelaer, O., Shao, H.-S., Stelzer, T., Torrielli, P., Zaro, M.: The automated computation of tree-level and next-to-leading order differential cross sections, and their matching to parton shower simulations. *JHEP* **07**, 079 (2014) [https://doi.org/10.1007/JHEP07\(2014\)079](https://doi.org/10.1007/JHEP07(2014)079) [arXiv:1405.0301](https://arxiv.org/abs/1405.0301) [hep-ph]
- [28] Frederix, R., Frixione, S., Hirschi, V., Pagani, D., Shao, H.-S., Zaro, M.: The automation of next-to-leading order electroweak calculations. *JHEP* **07**, 185 (2018) [https://doi.org/10.1007/JHEP11\(2021\)085](https://doi.org/10.1007/JHEP11(2021)085) [arXiv:1804.10017](https://arxiv.org/abs/1804.10017) [hep-ph]. [Erratum: *JHEP* 11, 085 (2021)]
- [29] Bierlich, C., Chakraborty, S., Desai, N., Gellersen, L., Helenius, I., Ilten, P., Lönnblad, L., Mrenna, S., Prestel, S., Preuss, C.T., Sjöstrand, T., Skands, P., Uthmeim, M., Verheyen, R.: A comprehensive guide to the physics and usage of PYTHIA 8.3 (2022)
- [30] Favereau, J., Delaere, C., Demin, P., Giammanco, A., Lemaître, V., Mertens, A., Selvaggi, M.: Delphes 3: a modular framework for fast simulation of a generic collider experiment. *Journal of High Energy Physics* **2014**(2) (2014) [https://doi.org/10.1007/jhep02\(2014\)057](https://doi.org/10.1007/jhep02(2014)057)
- [31] Selvaggi, M.: DELPHES 3: A modular framework for fast-simulation of generic collider experiments. *J. Phys. Conf. Ser.*

- 523**, 012033 (2014) <https://doi.org/10.1088/1742-6596/523/1/012033>
- [32] Mertens, A.: New features in Delphes 3. J. Phys. Conf. Ser. **608**(1), 012045 (2015) <https://doi.org/10.1088/1742-6596/608/1/012045>
- [33] Chollet, F., et al.: Keras. <https://keras.io> (2015)
- [34] Kingma, D.P., Ba, J.: Adam: A Method for Stochastic Optimization (2017). <https://arxiv.org/abs/1412.6980>
- [35] Coelho, C.N., Kuusela, A., Li, S., Zhuang, H., Ngadiuba, J., Aarrestad, T.K., Loncar, V., Pierini, M., Pol, A.A., Summers, S.: Automatic heterogeneous quantization of deep neural networks for low-latency inference on the edge for particle detectors. Nature Machine Intelligence **3**(8), 675–686 (2021) <https://doi.org/10.1038/s42256-021-00356-5>
- [36] FastML Team: Fastmachinelearning/hls4ml. <https://doi.org/10.5281/zenodo.1201549> . <https://github.com/fastmachinelearning/hls4ml>
- [37] Ghielmetti, N., *et al.*: Real-time semantic segmentation on FPGAs for autonomous vehicles with hls4ml. Mach. Learn. Sci. Tech. (2022) <https://doi.org/10.1088/2632-2153/ac9cb5> arXiv:2205.07690 [cs.CV]
- [38] Vasudevan, A., Anderson, A., Gregg, D.: Parallel Multi Channel Convolution using General Matrix Multiplication (2017). <https://arxiv.org/abs/1704.04428>
- [39] Benedikt, M., et al.: Future Circular Hadron Collider FCC-hh: Overview and Status (2022) arXiv:2203.07804 [physics.acc-ph]